

# High-performance micromachined gyroscope with a slanted suspension cantilever\*

Xiao Dingbang(肖定邦)<sup>†</sup>, Wu Xuezhong(吴学忠), Hou Zhanqiang(侯占强), Chen Zhihua(陈志华), Dong Peitao(董培涛), and Li Shengyi(李圣怡)

(Microsystem Laboratory, National University of Defense Technology, Changsha 410073, China)

**Abstract:** This paper presents a novel structure for improving the stability and the mechanical noise of micromachined gyroscopes. Only one slanted cantilever is used for suspension in this gyroscope, so the asymmetry spring and the thermal stress, which most micromachined gyroscopes suffer from, are reduced. In order to reduce the mechanical noise, the proof masses are designed to be much larger than in most micromachined gyroscopes. The gyroscope chip is sealed at 0.001 Pa vacuum. A gyroscope sample and its read-out circuit are fabricated. The scale factor of this gyroscope is measured as 57.6 mV/(deg/sec) with a nonlinearity better than 0.12% in a measurement range of  $\pm 100$  deg/sec. The short-term bias stability in 20 min is 60 deg/h.

**Key words:** micromachined gyroscope; slanted cantilever; proof mass

**DOI:** 10.1088/1674-4926/30/4/044012

**EEACC:** 7230; 8340

## 1. Introduction

High-performance gyroscopes are the most critical components in many applications, e.g., space navigation and guided weapons. Micromachined gyroscopes are more attractive due to their small size and low cost. That is why there is a persistent world-wide effort to improve their performance. Many decoupled gyroscope structures with complicated suspension beams and frames are designed to reduce the cross-coupling error<sup>[1-5]</sup>, and high- $Q$  tuning fork gyroscopes with large masses are designed to reduce the mechanical noise<sup>[6,7]</sup>. A “butterfly” gyroscope using a double-clamped beam with an asymmetric cross section shows attractive performance<sup>[8,9]</sup>.

To achieve sub-deg/h rate resolution, a vibratory gyroscope must have very high quality factors, large sense capacitances, large proof masses and a large drive amplitude<sup>[6]</sup>. Improving the stability is also very critical for high-performance gyroscopes, because most micromachined gyroscopes suffer from asymmetry spring and thermal stress, which are caused by the fabrication imperfection and the thermal expansion difference between the gyroscope structure and the substrate.

The gyroscope structure presented in this paper uses only one slanted cantilever for suspension. Without multi-suspension beams and anchors, this gyroscope does not suffer from the problems mentioned above. The dimensions of this gyroscope are increased for a large drive amplitude and large proof masses. The quality factors of the drive and sense modes are maximized by perforating the large proof masses and sealing the gyroscope chip at high vacuum. These advantages allow this gyroscope to theoretically achieve a bias stability better than 1 deg/h.

## 2. Structure design

The designed gyroscope includes a silicon structure and a Pyrex glass substrate (see Fig. 1). The silicon structure in-

cludes a slanted cantilever and two perforated masses at the end of the cantilever. A recess is fabricated on the substrate, with several electrodes on the bottom of the recess.

In this micromachined gyroscope, only one slanted cantilever is used for suspension, so the asymmetry spring caused by fabrication imperfection in many micromachined gyroscopes with multi-suspension beams is avoided. This arrangement also reduces the temperature expansion effects on the gyroscope, while increasing the drive amplitude. These advantages will result in the improvement of the gyroscope's mechanical noise and stability.

The drive mode is the anti-phase swing oscillation of the masses in the gyroscope plane, caused by the bending of the cantilever (see Fig. 2(a)). The sense mode is the anti-phase oscillation of the masses out of the gyroscope plane, caused by the torsion of the cantilever (see Fig. 2(b)).

The back view of this gyroscope is shown in Fig. 3. There are three electrodes under each proof mass. The drive electrodes, named Cd+ and Cd-, are used to excite the drive mode oscillation. The sense electrodes, named Cs+ and Cs-, are used to detect the sense mode oscillation of the proof masses.

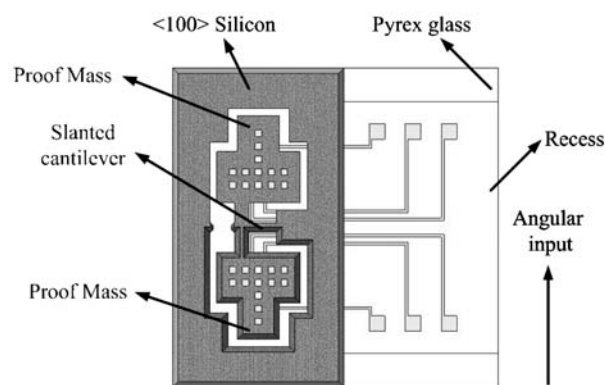


Fig. 1. View of the gyroscope structure.

\* Project supported by the National Natural Science Foundation of China (No. 50375154) and the NUDT Innovation Project for Excellent Postgraduates.

<sup>†</sup> Corresponding author. Email: Dingbangxiao@yahoo.com.cn

Received 10 October 2008, revised manuscript received 19 November 2008

© 2009 Chinese Institute of Electronics

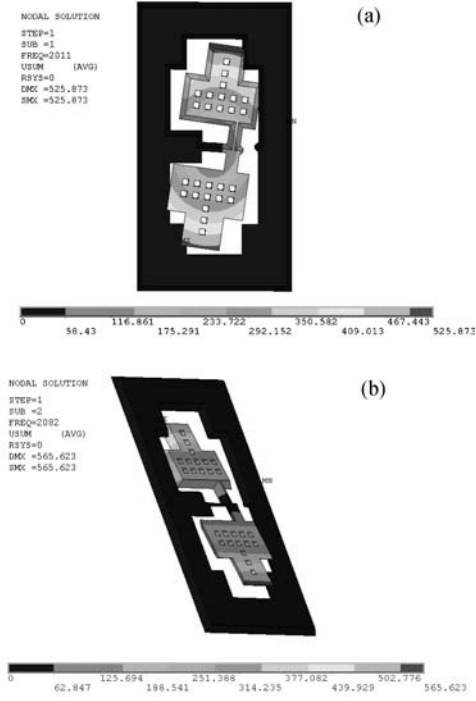


Fig. 2. (a) Drive mode; (b) Sense mode.

Suppose that the drive voltage applied on Cd+ is  $V_{d+}$ , and the drive voltage applied on Cd- is  $V_{d-}$ . The silicon structure is connected to ground.  $V_{d+}$  and  $V_{d-}$  are

$$\begin{cases} V_{d+} = D_d + A_d \sin \omega_d t, \\ V_{d-} = D_d - A_d \sin \omega_d t, \end{cases} \quad (1)$$

where  $D_d$  is the DC bias voltage, and  $\omega_d$  is the drive mode frequency.

The electrostatic forces generated by Cd+ and Cd- are (see Fig. 4)

$$\begin{cases} F_{e1} = \frac{C_{d0} V_{d+}^2}{h}, \\ F_{e2} = \frac{C_{d0} V_{d-}^2}{h}, \end{cases} \quad (2)$$

where  $C_{d0}$  is the static capacitance of a drive capacitor, and  $h$  is the distance between the drive electrode and the silicon structure.

The resultant force and moment of these electrostatic forces are

$$\begin{cases} F_e = F_{e1} + F_{e2} = \frac{C_{d0} (V_{d+}^2 + V_{d-}^2)}{h}, \\ M_e = (F_{e1} - F_{e2}) (W_d + W_1) = \frac{C_{d0} (V_{d+}^2 - V_{d-}^2) (W_d + W_1)}{h}, \end{cases} \quad (3)$$

where  $W_d$  is the width of the drive electrode, and  $W_1$  is the distance between Cd+ and Cd-. The direction of the moment is determined by the right-hand rule. By substituting Eq. (1) into Eq. (3), we find

$$\begin{cases} F_e = \frac{2C_{d0} (D_d^2 + A_d^2 \sin^2 \omega_d t)}{h}, \\ M_e = \frac{4C_{d0} D_d A_d (W_d + W_1) \sin \omega_d t}{h}. \end{cases} \quad (4)$$

Only forces or moments at the drive mode frequency could excite the gyroscope to resonance. There is no component at the

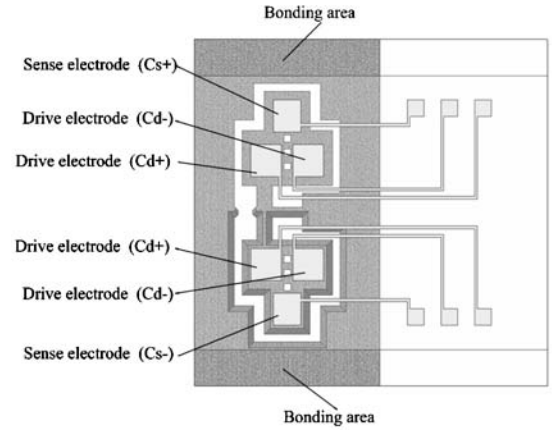


Fig. 3. Back view of this gyroscope.

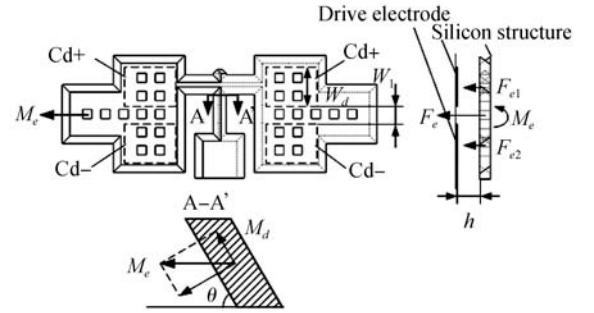


Fig. 4. Driving technique of this gyroscope.

drive mode frequency in the resultant force, so this gyroscope is excited by the electrostatic moment.

The dominating moment at the end of the slanted cantilever is shown on the cross section A-A' in Fig. 4. The projection of  $M_e$  in the bending direction of the drive mode is

$$M_d = M_e \cos \theta = \frac{4C_{d0} (W_d + W_1) D_d A_d \cos \theta \sin \omega_d t}{h}, \quad (5)$$

where  $\theta$  is the slanting angle of the cantilever.

$M_d$  bends the slanted cantilever, so the drive mode oscillation is generated.

### 3. Fabrication

The gyroscope was fabricated on n-type <100> silicon wafers with a resistivity of  $10^{-2} \Omega \cdot \text{cm}$ , and the electrodes are made on Pyrex #7740 glass wafers. Figure 5(a) shows the fabrication process. There are mainly five steps.

(1) The Pyrex glass wafer is etched in BOE with a recess of  $10 \mu\text{m}$  using Cr-Au masks.

(2) Aluminum electrodes are implemented on the bottom of the recess by sputtering, patterning and etching.

(3) The silicon wafer is patterned on both sides after oxidating.

(4) The silicon wafer is etched through in 25% TMAH at a temperature of  $90^\circ\text{C}$ , and then the silicon dioxide film is etched off in HF.

(5) The silicon wafer is bonded with the glass wafer, and the diced gyroscope chips are sealed in metal packages at 0.001 Pa vacuum.

The fabricated chip and the sealed gyroscope are shown in Fig. 5(b).

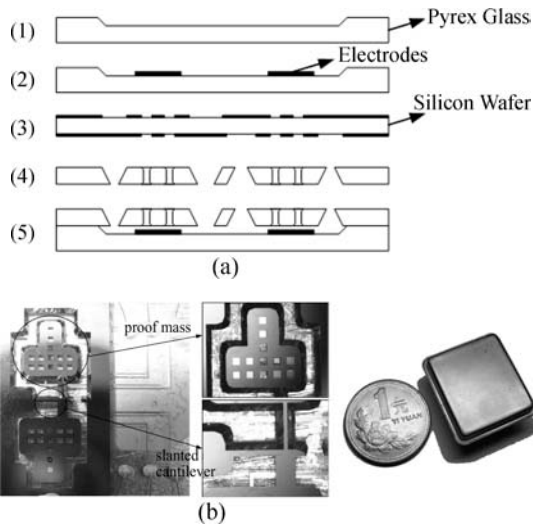


Fig. 5. (a) Fabrication process; (b) Fabricated chip and the packaged gyroscope.

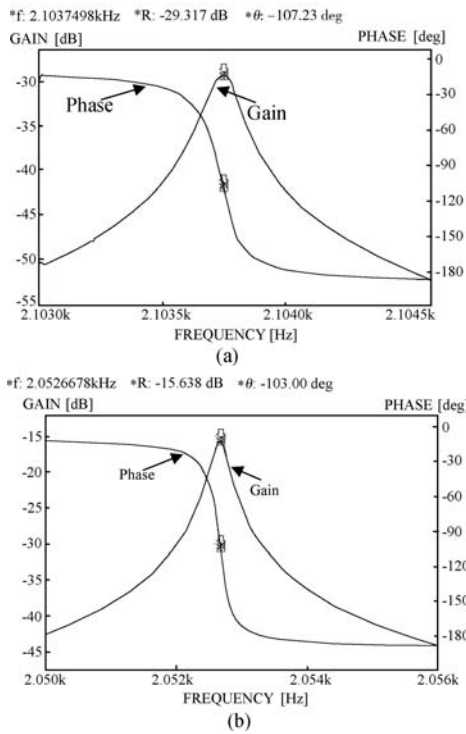


Fig. 6. (a) Frequency response of the drive mode; (b) Frequency response of the sense mode.

### 4. Characterization

The drive and sense modes are characterized by electrostatic excitation with a sinusoidal signal using a frequency sweep and simultaneous capacitive detection, using an NF frequency response analyzer FRA5087 (see Fig. 6). The resonance frequencies of the drive and sense modes are 2.104 and 2.053 kHz, and the quality factors of the drive and sense modes are 16830 and 8052, respectively.

Table 1 summarizes the key parameters of the fabricated gyroscope. According to Ref. [10], the thermo-mechanical equivalent rate signal of this gyroscope is

$$Q_n = \sqrt{\frac{k_B T \omega_s \Delta f}{m \omega_d^2 A_d^2 Q_s}} = 0.7562 \text{ deg/h}, \quad (6)$$

Table 1. Summary of the parameters of the fabricated gyroscope.

Silicon structure thickness	300 $\mu\text{m}$
Length of the slanted cantilever	1075 $\mu\text{m}$
Width of the slanted cantilever	Designed: 150 $\mu\text{m}$ Fabricated: 151 $\mu\text{m}$
Effective mass ( $m$ )	9 mg
Designed drive amplitude ( $A_d$ )	4 $\mu\text{m}$
Sealing vacuum	0.001 Pa
Drive mode resonant frequency ( $\omega_d$ )	Ansys: 2.011 kHz Measured: 2.104 kHz
Sense mode resonant frequency ( $\omega_s$ )	Ansys: 2.082 kHz Measured: 2.053 kHz
$\Delta f$	Measured: 51 Hz
$Q$ factor of drive mode ( $Q_d$ )	16830
$Q$ factor of sense mode ( $Q_s$ )	8052

Table 2. Measured  $Q$  factors of this gyroscope during three months.

Weeks	$Q$ factor of drive mode	$Q$ factor of sense mode
1st	16830	8052
2nd	17421	8137
3rd	17220	8104
4th	17332	8216
5th	16934	8097
6th	16431	8021
7th	16278	8004
8th	17586	8265
9th	17459	8204
10th	16962	8108
11th	17763	8292
12th	16873	8097

where  $K_B$  is the Boltzmann constant, and  $T$  is the temperature. This result means that this gyroscope can theoretically achieve a bias stability better than 1 deg/h at room temperature.

The  $Q$  factors of this gyroscope were measured weekly for three months, and the results are shown in Table 2. There was no distinct decrease of the  $Q$  factor during these months, and the variations of the  $Q$  factors are mainly due to measure errors. It can be concluded that the metal package of this gyroscope maintains the high inner vacuum very well.

The electrical model of the gyroscope is a capacitive pseudo-full bridge. In order to improve the stability of this high  $Q$  factor gyroscope, a closed-loop drive controller and a force balance controller are designed<sup>[8]</sup>. The block diagram of the readout circuit as well as the fabricated PCB, are shown in Fig. 7.

Figure 8 shows the output of this gyroscope versus the angular rate input in a measurement range of  $\pm 100$  deg/sec with 10 deg/sec steps. The gyroscope demonstrates a scale factor of 57.6 mV/(deg/sec). The nonlinearity of the measured scale-factor is 0.12% within the full measurement range.

Figure 9 shows the measured random noise of the output bias of this gyroscope for zero rate input. The short-term bias stability in 20 min is 60 deg/h. The drift of the zero-rate output is dominated by the phase error and the drift of the low-cost read-out electronics.

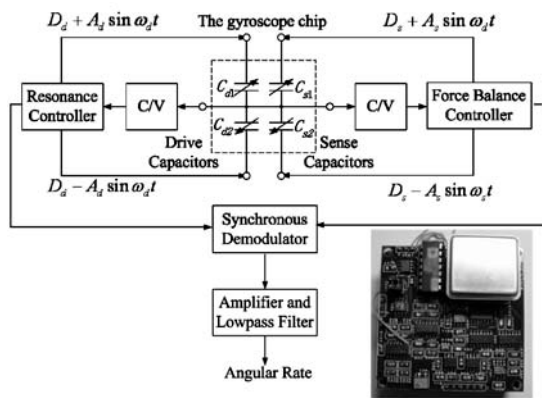


Fig. 7. Readout circuit of this gyroscope.

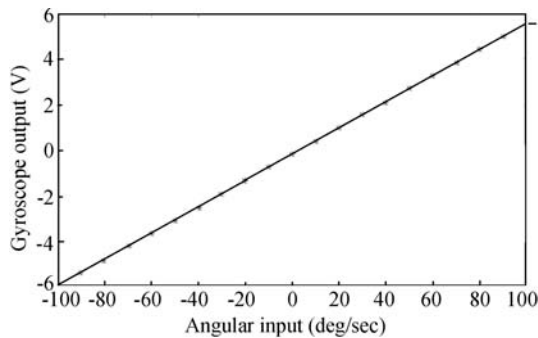


Fig. 8. Angular rate input versus voltage output plot obtained from the fabricated gyroscope.

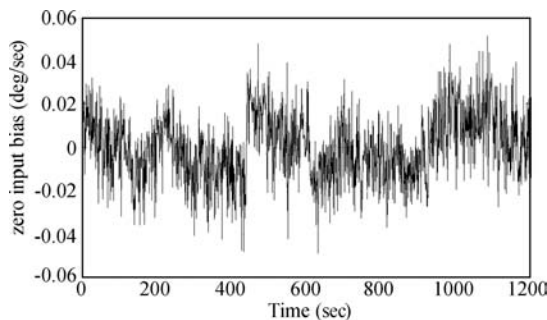


Fig. 9. Random variation of the output bias of the gyroscope for zero-rate input measured for 20 min.

### 5. Conclusions

A micromachined gyroscope with a slanted suspension cantilever was designed and fabricated. The gyroscope chip

was sealed in a metal package at 0.001 Pa vacuum. The resonance frequencies of the drive and sense modes are 2.104 and 2.053 kHz, and the quality factors of the drive and sense modes are 16830 and 8052 respectively. The scale factor of the gyroscope was measured as 57.6 mV/(deg/sec) with a nonlinearity better than 0.12% in a measurement range of ±100 deg/sec. The short-term bias stability in 20 min is 60 deg/h.

### References

- [1] Acar C, Shkel A. Structurally decoupled micromachined gyroscopes with post-release capacitance enhancement. *J Microelectromech Syst*, 2005, 15: 1092
- [2] Alper S E, Akin T. A single-crystal silicon symmetrical and decoupled MEMS gyroscope on an insulating substrate. *J Microelectromech Syst*, 2005, 14(4):707
- [3] Duan Fei, Jiao Jiwei, Wang Yucai, et al. A novel micromachined *x*-axis tuning fork gyroscope based on “8-beams/proofmass” structure. *Chinese Journal of Semiconductors*, 2007, 28(10):1630 (in Chinese)
- [4] Chen Yong, Jiao Jiwei, Wang Huiquan, et al. Design and noise analysis of a micromachined gyroscope working at atmospheric pressure. *Chinese Journal of Semiconductors*, 2005, 26(1):149 (in Chinese)
- [5] Li X, Chen X, Song Z, et al. A microgyroscope with piezoresistance for both high-performance coriolis-effect detection and seesaw-like vibration control. *J Microelectromech Syst*, 2006, 15(6): 1698
- [6] Sharma A, Zaman F M, Amini B V, et al. A high-*Q* in-plane SOI tuning fork gyroscope. 3rd IEEE International Conference on Sensors, Vienna, 2004: 467
- [7] Zaman M, Sharma A, Ayazi F. High performance matched-mode tuning fork gyroscope. 19th IEEE International Conference on MEMS, Istanbul, 2006: 66
- [8] Andersson G I, Hedenstierna N, Svensson P, et al. A novel silicon bulk gyroscope. 10th IEEE International Conference on Transducers, Sendai, 1999: 902
- [9] Hedenstierna N, Habibi S, Ilsen S M, et al. Bulk micromachined angular rate sensor based on the “butterfly” gyro structure. 14th IEEE International Conference on MEMS, Inter-laken, 2001: 178
- [10] Bao M H. *Micro mechanical transducers: pressure sensors, accelerometers and gyroscopes*. Amsterdam, Elsevier, 2000: 370